Interplay Between PEO Tether Length and Ligand Spacing Governs Cell Spreading on RGD-Modified PMMA-*g*-PEO Comb Copolymers

William Kuhlman,[†] Ikuo Taniguchi,[†] Linda G. Griffith,[‡] and Anne M. Mayes*[,†]

Department of Materials Science and Engineering, Massachusetts Institute of Technology, Cambridge, Massachusetts, 02139, and Department of Mechanical Engineering and Department of Biological Engineering, Massachusetts Institute of Technology, Cambridge, Massachusetts, 02139

Received February 27, 2007; Revised Manuscript Received July 17, 2007

The effects of tether length on cell adhesion to poly(methyl methacrylate)-*graft*-poly(ethylene oxide), PMMA-*g*-PEO, comb copolymer films functionalized with the adhesion peptide RGD were investigated. Copolymers having PEO tether lengths of 10 and 22 EO segments were synthesized and coupled with a synthetic peptide that contained both RGD and the synergy sequence PHSRN. Cell spreading assays revealed that the longer polymer tethers increased the rate of spreading and reduced the time required for fibroblasts to form focal adhesions. Fluorescence resonance energy transfer (FRET) measurements indicated a mean separation between integrin-bound peptides of 15.6 ± 1.4 nm for combs with long (22-mer) tethers, compared with 17.5 ± 1.3 nm for short (10-mer) tethers, on films of comparable peptide density (∼2500 peptides/μm^2). The results suggest that the added mobility afforded by the more extensible tethers encouraged the formation of focal adhesions by allowing cells to reorganize tethered peptides on the nanometer length scale. In addition, adhesion peptides were selectively coupled to 10-mer or 22-mer PEO tethers within a bimodal brush to investigate stratification effects on cell adhesion. Peptides bound by short tethers in a bed of long unsubstituted chains resulted in surfaces that resisted, rather than promoted, cell adhesion. By contrast, when long peptide tethers were employed with short unsubstituted chains, cell attachment and spreading were comparable to that found on a monomodal brush of long chains at equivalent peptide density.

Introduction

Materials presenting end-grafted poly(ethylene oxide) (PEO) chains functionalized with adhesion peptides are of interest as biomaterials because they show good resistance to nonspecific protein adsorption,[1] yet can engender strong cell attachment through adhesive moieties covalently bound to the free ends of some PEO chains.[2−7] Most such systems under investigation consist of two types of chains, each serving a different purpose: unsubstituted PEO chains that impart protein adsorption resistance, and peptide-functionalized "substituted" chains that promote receptor-mediated cell adhesion.[8−12] Experimental evidence suggests that the length and spacing of peptide-bearing chains influence receptor-mediated interactions with tethered ligands.[8,9,13,14] Many practical PEO tethering schemes employ brushes with a distribution of chain lengths for both ligand-substituted and unsubstituted components; hence, it remains of interest to disclose design principles for how tether length and spacing influence particular cell behaviors, using systems in which these parameters are systematically varied. Here, we illuminate how the interplay between the chain length and the spacing of peptide-conjugated PEO chains influences integrin-mediated cell attachment and spreading, including investigation of bimodal brush systems, in a tether length regime not previously examined. The results may be useful in the design of systems where dynamic integrin-mediated interactions (e.g., cell migration) are important.

Some insights into the effects of tether length on integrin receptor−ligand binding come from experimental[15,16] and theoretical[17,18] studies of receptor−ligand binding in systems of isolated molecular partners with well-characterized binding properties. Israelachvili and co-workers studied avidin binding to PEO-tethered biotin using a surface force apparatus. They found that tethering enhanced the activity of biotin by extending the minimum distance required to bind avidin-coated surfaces, from a natural distance of a few angstroms to a distance of several nanometers, corresponding to the fully extended length of the polymer tether.[15,16] These findings were further supported by numerical models.[17,18]

As with avidin−biotin interactions, integrin−peptide interactions occur over a short range, typically on the order of a nanometer.[19] Consequently, employing extensible chains to tether adhesion peptides may enhance cell attachment to cell-signaling polymer brushes. Beer et al., for example,[20] studied platelet adhesion to RGD-bearing polyacrylonitrile beads where the length of the polyglycine tether varied from 1 to 19 glycine units. They observed a maximum in bead adhesion to platelets for tethers of 9−15 units, suggesting spacers should be sufficiently long to permit ligand access to receptor binding sites, but short enough to allow fast binding kinetics.

Perhaps equally importantly, tether length may also govern cell responses subsequent to ligand binding by influencing the ability of bound integrins to spatially reorganize and cluster in the cell membrane. Integrin clustering is required to elicit a full range of biological responses,[19,21−23] and recent studies indicate that integrins exist in a pre-clustered state at the leading edge of migrating cells[24] and on the surface of dendritic cells,[25] perhaps priming integrins to interact with clustered adhesion

* Corresponding author. E-mail: amayes@mit.edu.
[†] Department of Materials Science and Engineering.
[‡] Department of Mechanical Engineering and Department of Biological Engineering.

10.1021/bm070237o CCC: $37.00 © 2007 American Chemical Society
Published on Web 09/18/2007

ligands in the extracellular environment. To induce integrin clustering, previous studies have employed nanometer-length scale clusters of adhesion peptides on surfaces.[10−12,14,26−28] For ligands bound by polymer tethers, longer tethers may enhance cell attachment by permitting integrin cluster formation through the larger number of available chain conformations.

Further increases in bioactivity may also be possible through the use of a bimodal polymer brush. When a polymer brush is composed of chains with two different lengths, short chains force the ends of long chains to the top of the brush layer, resulting in stratification of chain ends.[29−33] Embedding long ligand-bearing chains in a sea of short unsubstituted chains might thus be expected to enhance ligand availability by forcing them to the brush surface. This effect was seen experimentally by Houseman and Mrksich,[9] who prepared self-assembled monolayers of unsubstituted oligoethylene glycol (OEG) chains having three to six EG (or EO) units intermixed with RGD-conjugated hexaethylene glycol chains. They found that fibroblast adhesion to the RGD-bearing chains increased as the length of the unsubstituted OEG chains decreased. Similarly, Dori et al. studied melanoma cell adhesion to Langmuir−Blodgett films of PEO brushes of varying lengths embedded with synthetic peptide amphiphiles incorporating an adhesion ligand from type IV collagen.[13] For PEO brushes much shorter than the ligand-bearing amphiphiles (3 or 17 EO units), cell adhesion and spreading were observed; on PEO brushes of comparable length (∼45 EO units), cells adhered but did not spread; brushes substantially longer than the amphiphiles (∼114 EO units) showed no cell attachment, suggesting ligands were masked by the PEO chains. Polymer vesicles comprising bimodal PEO brushes functionalized with biotin have shown comparable trends in adhesion to avidin-coated surfaces.[34−36] Such behavior has also been predicted by Monte Carlo simulations of receptor binding to tethered ligands.[37]

Here, we investigate the inter-related effects of tether length and ligand spacing on cell attachment to surfaces bearing PEO-tethered ligands, by employing amphiphilic comb copolymers consisting of a hydrophobic poly(methyl methacrylate) (PMMA) backbone and hydrophilic PEO side chains of chosen lengths.[10,11,38] When exposed to an aqueous environment, comb molecules near the copolymer film surface arrange into quasi two-dimensional conformations in which PEO side chains extend into solution, while the PMMA backbone remains pinned at the interface.[10,39] The resulting dense PEO brush layer resists nonspecific protein adsorption and cell adhesion.[10−12,38,40,41] To induce integrin-mediated cell attachment, adhesion peptides are coupled to a defined fraction of the free PEO chain ends. We use a bifunctional peptide that consists of the primary recognition site for the $\alpha_5\beta_1$ integrin (GRGDSP) and the synergy peptide sequence PHSRN[42] presented in a branched conformation, with a GGC side chain suitable for covalently binding the peptide to a maleimide bearing surface, PHSRNGGGK(GGC)-GGRGDSPY (abbreviated here as PHSRN-K-RGD). Co-localization of these epitopes has been shown to greatly improve cell adhesion over linear RGD peptides for certain cell types.[43−46]

For these systems, we first examined the effects of overall tether length on cell attachment by preparing films of PMMA-*g*-PEO molecules with side chains of either 10 (EO_{10}) or 22 (EO_{22}) ethylene oxide segments. Adhesion peptides were coupled to these films to achieve an average ligand spacing estimated to be slightly greater than the distance between adjacent integrins in a focal contact, so that effects of tether length on integrin clustering might be discerned. Cell attachment was assessed by measuring cell spreading area and through immunochemical staining. The spatial organization of integrin-bound peptides was further examined using fluorescence resonance energy transfer (FRET) measurements. In addition, the effects of a bimodal length distribution of PEO chains in the brush layer were investigated by examining cell attachment and spreading on surfaces where peptide-substituted chains were either shorter, longer, or the same length as the unsubstituted chains.

Materials

Methyl methacrylate (MMA), PEO (M_n = 1000), methacryloyl chloride, ethanedithiol, triisopropylsilane, *N*,*N*′-diisopropylethylamine (DIPEA), 2,2′-azobis(2-methylpropionitrile) (AIBN), Hoechst 33258, and tetramethylrhodamine isothiocyanate (TRITC)-conjugated phalloidin (phalloidin-TRITC) were obtained from Aldrich Chemical Co. Dichloromethane, *N*-(*p*-maleimidophenyl) isocyanate (PMPI), Triton X-100, Chromerge, and phosphate buffered saline (PBS) were obtained from VWR Scientific. Siliclad was obtained from Gelest. Silicon wafers were obtained from University Wafers. Deionized water was produced using a Milli-Q water purification unit from Millipore. BioBeads were purchased from Bio-Rad. 9-Fluorenylmethyloxycarbonyl (FMOC) protected amino acids, NovaSyn TGR resin, *N*-hydroxybenzotriazole (HOBt), tris(2-carboxyethyl)phosphine (TCEP), and benzotriazole-1-yl-oxy-tris-pyrrolidino-phosphonium hexafluorophosphate (PyBOP) were purchased from NovaBiochem. Iodobeads were purchased from Pierce. $Na^{125}I$ was obtained from Perkin-Elmer. All chemicals were reagent grade and used as supplied unless otherwise noted. Trypsin, modified Eagles' medium-α, fetal bovine serum, nonessential amino acids, sodium pyruvate, L-glutamine, penicillin, streptomycin, and Geneticin G418 were obtained from Gibco. Tissue culture was performed using Falcon plates. Vybrant DiI cell-labeling solution stain, Alexa488 and Alexa546 were obtained from Molecular Probes. WTNR6 fibroblast cells, derived from the NIH3T3 cell line, were kindly provided by Professor Alan Wells at the University of Pittsburgh.

Methods

Macromonomer Synthesis. EO_{22} methacrylate macromonomer was synthesized by adding 0.15 equiv of methacryloyl chloride dropwise to a 30 wt % solution of PEO (1000 Da) and a 2-fold excess of triethylamine in dichloromethane, chilled in an ice bath (Figure 1a). The reaction was allowed to proceed overnight with stirring. The crude product was extracted once with 0.01 M hydrochloric acid, twice with brine, and finally once with deionized water. The product was dried over magnesium sulfate, and the solvent was removed by rotary evaporation. ^{1}H NMR (Bruker, DPX-400) showed the appearance of a new peak at $\delta = 4.29$ ppm, corresponding to the methylene protons of PEO adjacent to the methacrylate ester. ^{1}H NMR (400 MHz in $CDCl_3$), δ (ppm): 1.96 (s, 3H, CH_3), 3.44−3.82 (m, 86H, CH_2CH_2O), 4.29 (t, 2H, $COOCH_2$), 5.59 (s, 1H, CH═C), and 6.15 (s, 1H, CH═C).

Polymer Synthesis. PMMA-*g*-PEO comb copolymers with 10 EO segments per side chain (PMMA-*g*-EO_{10}) were synthesized by free-radical polymerization in toluene through a macromonomer route using AIBN as reported elsewhere (Figure 1b).[10] PMMA-*g*-EO_{22} was prepared by copolymerizing 17.6 g of the crude PEO derivative containing 4 mmol EO_{22} methacrylate macromonomer (22% purity) with 6.35 g of MMA (6.35 mmol) in 100 mL of ethanol using 30 mg of AIBN as an initiator at 65 °C overnight. The reaction mixture was precipitated in hexane, and the polymer was purified by size exclusion chromatography (BioBeads) using tetrahydrofuran as an eluent.

Molecular weights were determined using gel-permeation chromatography with in-line light scattering (Wyatt MiniDawn). The number-average molecular weight and polydispersity were M_n=142 kDa and PDI = 3.2 for PMMA-*g*-EO_{10}, and M_n = 510 kDa and PDI = 3.7 for

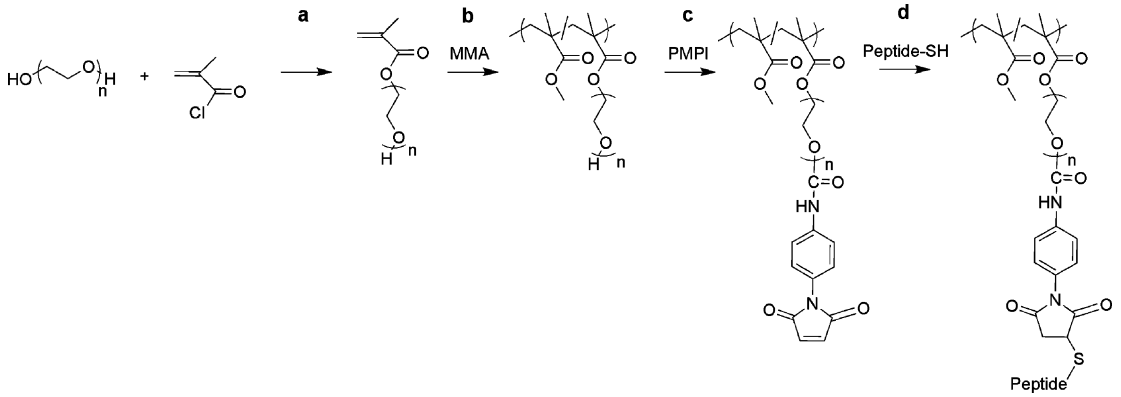

Figure 1. Synthesis of PEO macromonomer (a), synthesis of PMMA-*g*-PEO (b), reaction of PMMA-*g*-PEO with PMPI (c), and coupling of a thiol-bearing peptide to PMMA-*g*-PEO through PMPI (d).

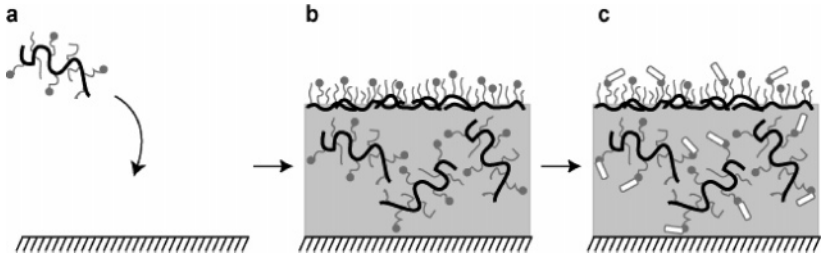

Figure 2. Schematic illustration of surface preparation. Surfaces are spin cast from PMPI-activated PMMA-*g*-PEO (a) and then exposed to peptide solution (b) to produce the peptide-bearing surface (c).

PMMA-*g*-EO_{22}. Polymer composition was determined by proton NMR (Bruker DPX, 400 MHz) in deuterated chloroform using previously reported peak assignments.[10] PMMA-*g*-EO_{10} and PMMA-*g*-EO_{22} contained 32 and 29 wt % PEO, respectively. These PEO contents are sufficiently high to resist cell adhesion, yet low enough to render the polymers water insoluble.[10]

PMPI Coupling. Defined fractions of PEO chain ends were functionalized with maleimide groups using PMPI, following the method of Annunziato et al. (Figure 1c).[47] The polymer was first lyophilized from benzene, and then redissolved in anhydrous dimethyl sulfoxide (DMSO). Two equivalents of PMPI relative to hydroxyl groups were added, and the reaction was allowed to proceed with mixing overnight at room temperature. Afterward, purification of the product was accomplished through repeated precipitation in diethyl ether. The product was characterized by proton NMR in deuterated DMSO. The degree of functionalization was determined by measuring the ratio of the peak at $\delta = 7.2$ ppm (s, 2H, maleimide) to the peak at 4.2 ppm (t, 2H, ester methylene). The fraction of coupled PEO chain ends on PMMA-*g*-EO_{10} and PMMA-*g*-EO_{22} was 60% and 80%, respectively.

Peptide Synthesis. The PHSRN-K-GRGDSP peptide was prepared following the method of Ufret and Griffith.[46] The linear portion, PHSRNGGGK(Mtt)GGRGDSPY, was synthesized on NovaSyn TGR resin using an Advanced Chem Tech 396 Ω peptide synthesizer following standard FMOC peptide synthesis methods.[48] DIPEA was used as an activating agent. PyBOP and HOBt were used to suppress racemization. The methoxytrityl (Mtt) protecting group of the lysine was subsequently removed using 1% trifluoroacetic acid (TFA) to yield a free amine. The GGC stem was then coupled to this amine using FMOC chemistry to obtain the Y-shaped peptide PHSRNGGGK(GGC)-GGRGDSPY (also referred to herein as PHSRN-K-GRGDSP). The resulting peptide was cleaved from the resin using TFA/triisopropylsilane/H_2O/ethanedithiol ratios of 92.5:2.5:2.5:2.5, and was reprecipitated in cold ether several times. The peptide was then lyophilized and subsequently purified using a YMC AQ1S05 reverse-phase column on a Waters Breeze HPLC system, running acetonitrile and water with 0.1% TFA as eluents. Composition was verified by mass spectrometry (Agilent). PHSRN-K-GRGDSP peptides used in radiolabeling studies were iodonated following the iodobead method[49] and purified on Sep-Pack C-18 columns (Waters).

Table 1. Surface Concentrations of Peptides Used for Studies on Homogeneous Brushes Composed Entirely of PMPI-Coupled Polymer, and Blend Brushes Composed of 25 wt % PMPI-Coupled Polymer with Side Chains of n_s EO Segments and 75 wt % Unsubstituted Polymer Having Side Chains of n_u EO Segments

composition	n_s	n_u	peptides/10^{-3} μm^2
homogeneous	10		2.89 ± 0.17
	22		2.11 ± 0.88
blend	10	22	1.77 ± 0.46
	22	10	2.56 ± 0.81
	10	10	2.85 ± 0.59
	22	22	2.36 ± 0.52

Surface Preparation. Glass coverslips were soaked overnight in Chromerge, rinsed with deionized water, treated for 30 s with a 2% aqueous solution of Siliclad, rinsed again with deionized water, and finally cured in an oven at 100 °C for 5 min. Films of PMPI-coupled PMMA-*g*-PEO were spin coated onto the treated coverslips from 1 wt % solution in toluene (Figure 2a). Thickness was determined by ellipsometry (Gartner L125A) on silicon wafers treated similarly. Films were annealed at 65 °C in vacuum overnight prior to peptide coupling. Peptide was coupled to the polymer by exposing the films to a PBS solution containing PHSRNGGGK(GGC)GGRGDSPY peptide and 10 μM of TCEP at pH 7.5 for 2 h to effect the coupling between the maleimide group on PMPI-modified chains and the thiol group on the GGC stem of the peptide (Figure 2b). Peptide coupling concentrations were adjusted in the range of 1−4 μM to achieve comparable peptide densities (~2500 peptides/μm^2) on brushes of varying RGD-substituted and unsubstituted chain lengths (Table 1). Following coupling, surfaces were rinsed twice with PBS and once with deionized water.

The surface density of the peptide was determined using ^{125}I-labeled peptides. Background arising from adsorbed, uncoupled peptide was measured from a film of PMMA-*g*-PEO not reacted with PMPI and subtracted from all subsequent measurements to ensure that only the surface density of covalently bound peptides was measured. Radiolabeling measurements on polymer films of different thicknesses indicated

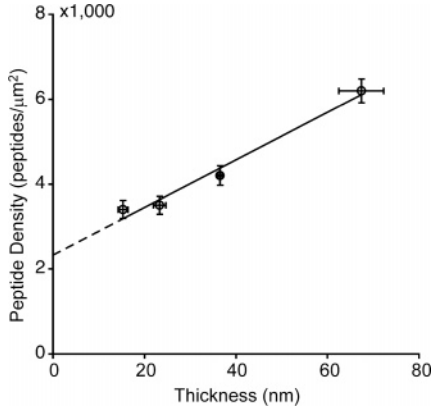

Figure 3. Variation in peptide density with PMMA-*g*-PEO film thickness observed by radiolabeling.

Table 2. Surface Concentration and Fraction of Total Peptides Coupled to Alexa488 and Alexa546 on Polymers Having Side Chains of *n* EO Segments used in FRET Measurements

chromophore	*n*	molecules/10^{-3} μm^2	fraction coupled
Alexa488	10	1.20 ± 0.15	0.41
	22	1.00 ± 0.14	0.47
Alexa546	10	0.73 ± 0.20	0.25
	22	0.66 ± 0.70	0.31

that the peptide was able to react with maleimide groups buried within the film as well as those at the surface. To estimate the peptide coverage only on the film surface, total peptide densities were determined for films of different thicknesses, ranging from 15 to 70 nm, and the data were extrapolated to zero thickness (Figure 3).

Substrates for FRET Measurements. Alexa488 and Alexa546 chromophores used in FRET measurements were attached by reacting a 100 μM solution of the NHS ester of each chromophore with the N-terminus of PEO-tethered peptides in 0.1 M sodium bicarbonate (pH 8.5) for 4 h, followed by rinsing twice with PBS and once with deionized water.[50] The extent of peptide coupling was determined by observing the intensity of each chromophore in the fluorescence microscope and comparing it to standards of known concentration. Results are given in Table 2.

Cell Culture. All surfaces were sterilized for 20 min with UV light prior to use in cell culture, except surfaces for FRET experiments, which were prepared in a sterile cell culture hood. Cell culture media consisted of modified Eagle's medium-α supplemented with 7.5% fetal bovine serum, 1% nonessential amino acids, 1% sodium pyruvate (100 mM), 1% L-glutamine (200 mM), 1% penicillin (10 000 U/mL), 1% streptomycin (10 mg/mL) and 35 mg/mL Geneticin G418. Confluent WTNR6 fibroblast cells (passage 10−15) were detached from tissue culture plates using trypsin and were suspended in media. The concentration of cells was determined using a Coulter Counter (Beckmen), and the suspension was diluted to 10 000 cells/mL with media. Two milliliters were then added to each well of a 12-well plate, containing a polymer-coated coverslip. PMMA-*g*-PEO control substrates, to which no peptides were coupled, were included in each trial and showed no cell attachment. Additionally, control surfaces functionalized with branched peptides having the RGD site scrambled to RDG did not support cell attachment.

Cell Attachment. Cells seeded on each substrate were allowed to attach for 45, 90, 135, or 180 min, then were fixed with a 3.7% formaldehyde solution in PBS. Cell nuclei were subsequently stained for 15 min with 1 μg/mL Hoechst 33258 in PBS, and the surfaces were then rinsed twice with PBS. Coverslips were mounted on microscope slides and imaged in a fluorescence microscope (Zeiss Axioskop). Cells were counted using ImageJ software (NIH).

Cell Spreading. Cells were allowed to attach for 30 min, and were then washed with PBS supplemented with calcium and magnesium. Fresh media were added, and the surfaces were returned to the incubator. Samples were taken at 30 min intervals and fixed with 3.7% formaldehyde solution in PBS. To determine the cell spreading area, cell membranes were stained with 0.5% DiI for 15 min in PBS at 36 °C, and the surfaces were then rinsed twice with PBS. Coverslips were mounted on microscope slides and imaged in a fluorescence microscope (Zeiss Axioskop). Individual cells were identified, and their areas were determined using ImageJ software (NIH). Samples were blinded to reduce operator bias.

Actin Fiber Staining. Cells were incubated on polymer substrates for 30, 90, or 150 min. Adherent cells were fixed with 3.7% formaldehyde, dried with acetone, permeabilized with 0.1% Triton X-100, and washed with PBS. Cells were then treated with 50 μg/mL phalloidin-TRITC to stain for actin fibers for 40 min at room temperature, followed by two additional PBS washes. Coverslips were mounted on microscope slides and imaged with a fluorescence microscope (Zeiss Axioskop).

FRET Measurements. FRET measurements were performed on a Zeiss Axioskop equipped with an AxioCam HR digital camera. The FRET filter set consisted of a dichroic mirror (Chroma 505DCLP), fluorescein isothiocyanate (FITC) excitation filter (Chroma D470/40), and a rhodamine emission filter (Chroma HQ610/75). Spectral bleed-through was corrected following the method outlined by Gordon et al.[51] by subtracting images obtained using an FITC (Zeiss Filter Set 09) or rhodamine (Zeiss Filter Set 15) filter set, each scaled by an empirically determined bleed-through constant. Contributions to the FRET signal from cell autofluorescence were corrected by subtracting the mean cell intensity measured using the FRET filter from cells on substrates with no chromophores. The distance (r) between chromophores was estimated from[51]

$$E = \frac{R_0^6}{R_0^6 + r^6} \tag{1}$$

where E is the resonance transfer energy, determined by multiplying the observed FRET intensity by an empirically determined transfer constant, and R_0 is the Förster radius for Alexa488/Alexa546 (5.5 nm).[52] Negative controls on which there were no chromophores did not show significant FRET.

Results and Discussion

Cell Attachment to Homogeneous Monomodal Brushes. To examine the effects of PEO tether length on cell attachment behaviors, cell spreading and FRET studies were performed to compare the attachment of fibroblasts on peptide-bearing PMMA-*g*-PEO surfaces of different PEO side chain lengths. Comb copolymers with 10 and 22 EO units per side chain, corresponding to contour lengths of 6.5 and 14.3 nm, respectively, were synthesized and cast into films. A fraction of the PEO side chains was functionalized with the branched peptide PHSRN-K-GRGDSP. We found that when the film thickness was increased from 15 to 70 nm, the amount of peptide covalently bound to the film per square micron also increased systematically (Figure 3). This result is attributed to the diffusion of peptides into the hydrated films and binding to maleimide groups within the films over the 2 h reaction period. To estimate the density of peptides available for cell interactions at the film surface, these data were extrapolated to zero film thickness. Reaction concentrations were then varied to achieve surface peptide densities of ~2500 peptides/μm^2, corresponding to an average equilibrium spacing between peptides of ~20 nm. While the spacing between adjacent integrins in various types of functional clusters (e.g., focal contacts and focal adhesions) is not precisely known, the chosen average peptide spacing of 20

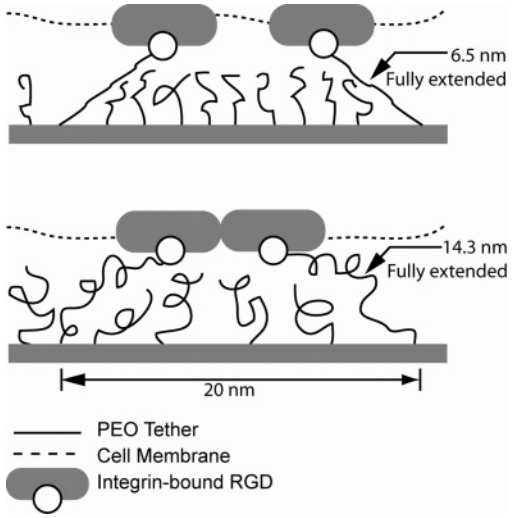

Figure 4. Schematic illustration of integrins interacting with PHSRN-K-GRGDSP peptide-coupled amphiphilic comb surfaces with 10-mer (top) and 22-mer (bottom) PEO side chains.

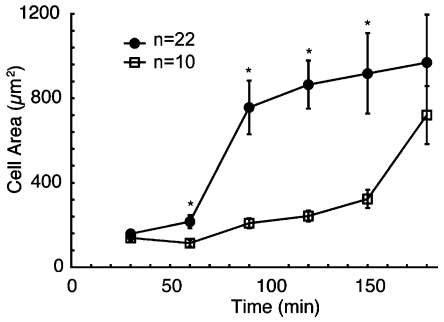

Figure 5. Cell spread area on PHSRN-K-GRGDSP-coupled surfaces of PMMA-*g*-PEO with 10-mer (squares) and 22-mer (circles) PEO side chains. $*p < 0.01$

nm is about twice the dimension of an integrin head.[19,53,54] At this peptide density, integrins bound to peptides attached by 10-mer PEO tethers will likely be constrained from forming close-neighbor aggregates (on average), even when tethers are fully extended (Figure 4). Integrins bound to peptides on 22-mer tethers, by contrast, should be able to form close-neighbor associations when the tethers are highly extended.

Figure 5 shows a comparative time course of cell spreading on surfaces made from PMMA-*g*-EO_{10} and PMMA-*g*-EO_{22}. The evolution of the intracellular organization of actin during spreading is shown in Figure 6. On both substrates, little evidence of cell spreading or actin stress fibers is seen at times less than 1 h. Cells plated on substrates presenting peptides bound by the more extensible 22-mer PEO tethers form focal adhesions and begin to spread within 90 min after plating, while those bound to the 10-mer tethers remain predominantly rounded. By 150 min after plating, however, cells binding to both surfaces show similar degrees of spreading and similar organization of actin. We attribute the faster spreading on PMMA-*g*-EO_{22} substrates to the increased ability of cells on these substrates to aggregate integrins by displacing adhesive ligands from their average ~20 nm spacing to create local clusters.[21,24]

In studies of fibroblast spreading on fibronectin, Dubin-Thaler et al. reported that the lag time for the initiation of cell spreading decreased with increasing surface fibronectin density, and suggested that spreading initiation might be viewed as a cellular "phase change" that occurred after the cell crossed a threshold of integrin signaling.[55] Integrin signaling requires integrin

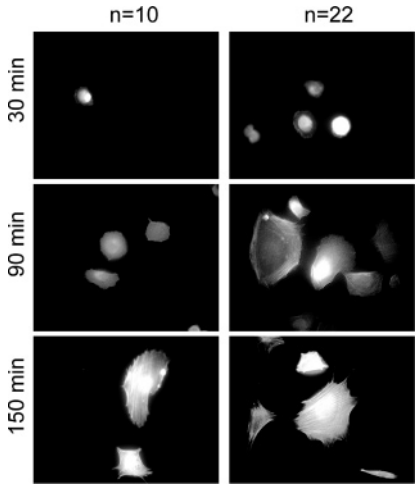

Figure 6. Actin staining of cells adhering to PHSRN-K-GRGDSP coupled to surfaces of PMMA-*g*-PEO with 10-mer (left) and 22-mer (right) PEO side chains at different incubation time points.

clustering,[21] hence, the initiation of spreading may require the formation of a threshold quantity of integrin clusters. For substrates coated with fibronectin by adsorption at low and moderate densities, molecules are distributed stochastically on the surface, and thus some molecules are intrinsically clustered. The probability of finding a cluster decreases with decreasing fibronectin density. During adhesion (and spreading), cells sample the surface, forming and breaking integrin−matrix bonds dynamically. Because many more binding and unbinding events are required to find a threshold quantity of statistically clustered ligands on a sparsely coated surface, reaching the threshold quantity of clustered, bound integrins required to initiate spreading is expected to take longer.[56,57]

In our studies, the average surface density of an adhesion peptide is the same on EO_{10} and EO_{22} surfaces, but because of the greater extensibility of EO_{22} tethers, we expect that the EO_{22} surfaces present a greater number of functional adhesion peptide clusters, because bound integrins can move tethered peptides sufficient lateral distances to allow integrin aggregates to form (Figure 4). For much longer tethers, we might expect the advantage of added extensibility to be outweighed by a reduction in binding kinetics due to the sampling of a larger number of available brush conformations, such that an optimum tether length exists for promoting cell adhesion dynamics, as found by Beer et al.[20]

To more directly address the possibility of cell-induced movement of tethered peptides, FRET measurements were conducted on surfaces in which PEO-tethered peptides were randomly labeled with Alexa488 or Alexa546. For the surface density of peptides used (~2500 total peptides/μm^2), donor- and acceptor-labeled peptides are separated by more than 20 nm on both comb surfaces. This distance is more than 3 times the Förster radius for this chromophore pair, and therefore little FRET is observed on either surface in the absence of cells. When fibroblasts attach, a dramatic increase in FRET is observed. Figure 7 shows bright field images and maps of average chromophore pair separation calculated from FRET data obtained from each comb surface after 3 h of incubation. Bright field images of the two surfaces show adherent cells with similar morphologies and spread areas (some rounded cells are also observed on EO_{10} surfaces). Donor−acceptor separations calculated on the basis of FRET, however, show a measurable difference in cells with similar morphologies (Figure 7c), with cells adhering to peptides bound by long tethers showing a

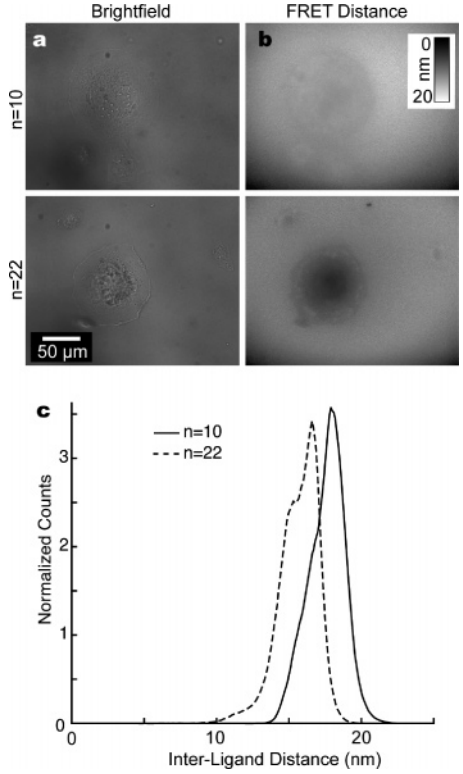

Figure 7. Bright field images (a) and ligand spacing calculated from FRET measurements (b) for PHSRN-K-GRGDSP coupled to PMMA-*g*-PEO polymers with 10-mer and 22-mer PEO side chains. (c) A histogram of bound interligand spacing.

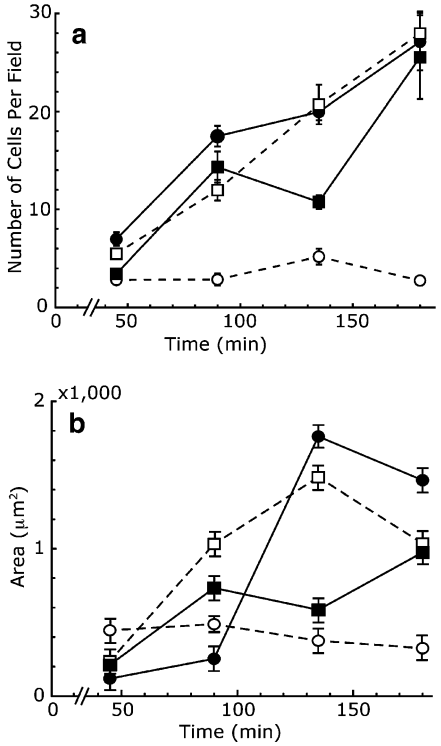

Figure 8. (a) Cell attachment and (b) spreading on surfaces made from a 25 wt % PMPI-coupled comb blended with an unsubstituted comb. PEO side chain lengths of RGD- substituted and unsubstituted combs varied. Closed circles: $n_s = 22$ blended with $n_u = 10$. Open squares: $n_s = 22$, n_u=22. Closed squares: $n_s = 10$, $n_u = 10$. Open circles: $n_s = 10$, $n_u = 22$.

smaller separation between bound ligands. A mean separation of 15.6 ± 1.4 nm was observed for chromophores on PMMA-*g*-EO_{22}, while a separation of 17.5 ± 1.3 nm was found for PMMA-*g*-EO_{10} (sample size: 30 cells per surface; statistically significant at $p = 0.05$). Peptides tethered by the longer PEO chains thus appear to be more readily repositioned laterally to accommodate receptor clustering.

The observed FRET intensity might alternatively be explained by micron-scale deformation of the polymer film. Cells can exert significant traction forces on their substrate, and cell-induced deformation has been reported for hydrogel substrates.[58] However, two observations suggest that micron-scale cell-induced deformation of the PMMA-*g*-PEO film substrates does not occur in our systems. First, fluorescence depletion rings around cells that would indicate micron-scale rearrangement of the polymer are absent. Second, when cells are removed from the films using trypsin, the resulting substrates show uniform fluorescence intensity, suggesting that no permanent deformation occurred. Both observations support the premise that the observed FRET increase in the presence of cells was due to rearrangement of peptide-bound integrins.

We note that the average ligand spacing where we observe these effects, 20 nm, is significantly smaller than the 58 nm spacing reported by Cavalcanti-Adam et al. to affect cytoskeletal organization of fibroblasts when single RGD ligands are presented at precise spacings.[14] We used a different RGD peptide, a different substrate, and a different cell line, and imaged cells within the first 3 h rather than after 24 h, as was done in that study. These factors and others could contribute to the difference in ligand spacing found to induce the measured cell responses in each case. Our FRET data indicate that integrins have a propensity to cluster with spacings less than 20 nm, at least in the early stages of cell spreading. The precise spacing between integrins in adherent cells is not known, and may vary substantially depending on the cell, the integrin, and the particular type of integrin−cytoskeletal contact associated with adhesion. Integrin clustering on <20 nm length scales has been observed for the integrin LFA-1 on the surface of monocytes,[25] and electron micrographs of activated integrins[54] support the inference that multiple integrin heads could pack into a 20 nm × 20 nm space.

Cell Attachment and Spreading on Blend and Bimodal Brushes. To examine the effects of chain length distribution on ligand accessibility, cell attachment and spreading assays were performed on peptide-coupled surfaces of films composed of blends of 25% PMPI-functionalized PMMA-*g*-PEO of a given PEO chain length (n_s), with unsubstituted PMMA-*g*-PEO of PEO chain length n_u. Surfaces with both 22-mer RGD-bearing chains blended with 10-mer unsubstituted chains and 10-mer RGD-bearing chains blended with 22-mer unsubstituted chains were examined and compared with control blends having components of identical length (10 or 22 EO units).

Figure 8 compares cell attachment (a) and spreading (b) on each of the four comb blend surfaces as a function of incubation time. Both control blends showed good cell attachment, with an overall increase in cell number and spreading over time. Bimodal brushes in which unsubstituted chains were longer than RGD-substituted chains, by comparison, showed little cell attachment and poor spreading, even after 3 h. For this system, unsubstituted chains effectively masked peptides attached to shorter chains, making the surface non-adhesive to cells. These findings are consistent with the results of Dori et al.[13] and with the surface force apparatus experiments by Moore and Kuhl, who observed a decrease in adhesive force between an avidin-coated surface and 45-mer biotinylated PEO chains in the presence of longer (114-mer) unsubstituted PEO chains.[36] In those systems, unsubstituted PEO chains were ~70 EO units

longer than substituted chains, versus 12 EO units in the present study. The pronounced effect of brush bidispersity on cell adhesion despite this small difference in chain lengths in our study may be attributed to the weak binding energy of integrin−RGD bonds (∼1−5 k_BT)[59] which can be overcome using a smaller steric barrier compared to avidin−biotin bonds (∼34 k_BT).[60,61]

For bimodal brushes in which RGD groups are tethered to 22-mer PEO chains, cell attachment and spreading are comparable to that of a monomodal 22-mer brush of comparable peptide density (Figure 8). No improvement in cell attachment is observed, beyond the previously noted difference between 10- and 22-mers found for monomodal brushes (Figure 8a). As seen in Figure 8b, blends with $n_s = 22$ RGD-substituted chains showed a dramatic increase in cell spreading around 130 min, while the monomodal $n_s = 10$ brush showed comparable spreading only after 3 h of incubation time. For the bimodal blend, stratification of chain ends to the top of the brush caused by a difference of 12 EO units appears insufficient to produce an observable enhancement in cell attachment or spreading over a 22-mer monomodal brush of comparable RGD substitution. Our data are inconsistent with experimental observations by Houseman and Mrksich,[9,62] Dori et al.,[13] and Hammer and coworkers,[34] as well as the simulation results of Chen and Dormidontova.[37] These studies all found enhanced receptor−ligand binding on bimodal brushes in which ligands were attached to long tethers vs monomodal brushes. However, our findings are in accord with the theoretical results of Longo and Szleifer, who predicted ligand−receptor binding for bimodal PEO brushes with 100-mer ligand-bearing chains and 25-mer unsubstituted chains to be comparable to that for 100-mer monomodal brushes of equal ligand density.[17] The diversity of behaviors reported across these studies may reflect differences in the range of tether lengths and ligand densities investigated.

Conclusions

This study demonstrated that increasing the length of PEO tethers used to attach RGD adhesion peptides to a polymer brush increases the rate of cell spreading and permits the formation of focal adhesions at shorter incubation times. FRET measurements suggest that the observed enhancement in cell adhesion kinetics is most likely due to the added mobility afforded by longer tethers, which facilitates nanoscale rearrangement of surface-bound peptides and promotes integrin clustering. Hence, the use of long tethers (i.e., whose extended length permits lateral ligand overlap) appears to be an effective strategy to promote the formation of integrin clusters.

Bimodal brushes composed of short (10-mer) RGD-substituted chains and long (22-mer) unsubstituted chains showed a dramatic decrease in cell attachment and spreading relative to those surfaces where RGD-substituted chains were of length equal to or greater than unsubstituted chains, consistent with the screening of adhesion peptides by the longer chains. Such a structure may be of value in designing targeted drug-delivery vehicles with surface-tethered functional groups selectively masked to reduce toxicity or prolong lifetime in vivo.[35,63] In contrast, ligand accessibility was not enhanced by a bimodal brush with shorter unsubstituted chains. For this case, adhesive properties were similar to those of a monomodal brush of long polymer tethers, suggesting that a bimodal brush affords little advantage in the chain length and ligand density regime investigated.

Acknowledgment. This work was funded by NIH Grant #1R0GM59870-01 and U54-GM064346. This work made use of the Shared Experimental Facilities supported by the MRSEC Program of the National Science Foundation under award number DMR 02-13282, and facilities supported by NIH grant 1S10RR13886-01. We would like to thank Daniel Pregibon, Dr. Maria L. Ufret, and Prof. Metin H. Acar for their assistance with synthesis.

References and Notes

(1) Harris, J. M. *Poly(ethylene glycol) Chemistry: Biotechnical and Biomedical Applications*; Plenum Press: New York, 1992.
(2) Nath, N.; Hyun, J.; Ma, H.; Chilkoti, A. *Surf. Sci.* **2004**, *570*, 98−110.
(3) Hersel, U.; Dahmen, C.; Kessler, H. *Biomaterials* **2003**, *24*, 4385−4415.
(4) Andrés, J. G. *Adv. Polym. Sci.* **2006**, *203*, 171−190.
(5) Otsuka, H.; Nagasaki, Y.; Kataoka, K. *Curr. Opin. Colloid Interface Sci.* **2001**, *6*, 3−10.
(6) Zhang, Z.; Yoo, R.; Wells, M.; Beebe, T. P., Jr.; Biran, R.; Tresco, P. *Biomaterials* **2005**, *26*, 47−61.
(7) Lutolf, M. P.; Hubbell, J. A. *Nat. Biotechnol.* **2005**, *23*, 47−55.
(8) Griffith, L. G.; Lopina, S. *Biomaterials* **1998**, *19*, 979−986.
(9) Houseman, B. T.; Mrksich, M. *Biomaterials* **2001**, *22*, 943−955.
(10) Irvine, D. J.; Mayes, A. M.; Griffith, L. G. *Biomacromolecules* **2001**, *2*, 85−94.
(11) Irvine, D. J.; Ruzette, A.-V. G.; Mayes, A. M.; Griffith, L. G. *Biomacromolecules* **2001**, *2*, 545−556.
(12) Koo, L. Y.; Irvine, D. J.; Mayes, A. M.; Lauffenburger, D. A.; Griffith, L. G. *J. Cell Sci.* **2002**, *115*, 1424−1433.
(13) Dori, Y.; Bianco-Peled, H.; Satija, S. K.; Fields, G. B.; McCarthy, J. B.; Tirrell, M. *J. Biomed. Mater. Res.* **2000**, *50*, 75−81.
(14) Cavalcanti-Adam, E. A.; Volberg, T.; Micoulet, A.; Kessler, H.; Geiger, B.; Spatz, J. *Biophys. J.* **2007**, *92*, 2964−2974.
(15) Wong, J. Y.; Kuhl, T. L.; Israelachvili, J. N.; Mullah, N.; Zalipsky, S. *Science* **1997**, *275*, 820−822.
(16) Jeppesen, C.; Wong, J. Y.; Kuhl, T. L.; Israelachvili, J. N.; Mullah, N.; Zalipsky, S.; Marques, C. M. *Science* **2001**, *293*, 465−468.
(17) Longo, G.; Szleifer, I. *Langmuir* **2005**, *21*, 11342−11351.
(18) Moreira, A. G.; Marques, C. M. *J. Chem. Phys.* **2004**, *120*, 6229−6237.
(19) Hynes, R. O. *Cell* **2002**, *110*, 673−687.
(20) Beer, J. H.; Springer, K. T.; Coller, B. S. *Blood* **1992**, *79*, 117−128.
(21) Miyamoto, S.; Akiyama, S. K.; Yamada, K. M. *Science* **1995**, *267*, 883−885.
(22) Yauch, R. L.; Felsenfeld, D. P.; Kraeft, S.-K.; Chen, L. B.; Sheetz, M. P.; Hemler, M. E. *J. Exp. Med.* **1997**, *186*, 1347−1355.
(23) Laplantine, E.; Maurer, P.; Vallar, L.; Eble, J.; Paulsson, M.; Bruckner, P.; Kieffer, N.; Aumailley, M. *Biol. Cell* **2002**, *94*, 375−387.
(24) Galbraith, C. G.; Yamada, K. M.; Galbraith, J. A. *Science* **2007**, *315*, 992−995.
(25) Cambi, A.; Joosten, B.; Koopman, M.; de Lange, F.; Beeren, I.; Torensma, R.; Fransen, J. A.; Garcia-Parajo, M.; van Leeuwen, F. N.; Figdor, C. G. *Mol. Biol. Cell* **2006**, *17*, 4270−4281.
(26) Maheshwari, G.; Brown, G.; Lauffenburger, D. A.; Wells, A.; Griffith, L. G. *J. Cell Sci.* **2000**, *113*, 1677−1686.
(27) Danilov, Y. N.; Juliano, R. L. *Exp. Cell Res.* **1989**, *182*, 186−196.
(28) Lee, K. Y.; Alsberg, E.; Hsiong, S.; Comisar, W.; Linderman, J.; Ziff, R.; Mooney, D. *Nano Lett.* **2004**, *4*, 1501−1506.
(29) Milner, S. T.; Witten, T. A.; Cates, M. E. *Macromolecules* **1989**, *22*, 853−861.
(30) Dan, N.; Tirrell, M. *Macromolecules* **1993**, *26*, 6467−6473.
(31) Chakrabarti, A.; Toral, R. *Macromolecules* **1990**, *23*, 2016−2021.
(32) Kent, M. S.; Factor, B. J.; Satija, S.; Gallagher, P.; Smith, G. S. *Macromolecules* **1996**, *29*, 2843−2849.
(33) Levicky, R.; Koneripalli, N.; Tirrell, M.; Satija, S. K. *Macromolecules* **1998**, *31*, 2616−2621.
(34) Lin, J. J.; Silas, J. A.; Bermudez, H.; Milam, V. T.; Bates, F. S.; Hammer, D. A. *Langmuir* **2004**, *20*, 5493−5500.
(35) Kim, D. H.; Klibanov, A. L.; Needham, D. *Langmuir* **2000**, *16*, 2808−2817.
(36) Moore, N. W.; Kuhl, T. L. *Langmuir* **2006**, *22*, 8485−8491.
(37) Chen, C.-C.; Dormidontova, E. E. *Langmuir* **2005**, *21*, 5605−5615.
(38) Walton, D. G.; Soo, P. P.; Mayes, A. M.; Allgor, S. J. S.; Fujii, J. T.; Griffith, L. G.; Ankner, J. F.; Kaiser, H.; Barker, J. G.; Satija, S. K. *Macromolecules* **1997**, *30*, 6947−6956.

(39) Kuhlman, W. A.; Olivetti, E. A.; Griffith, L. G.; Mayes, A. M. *Macromolecules* **2006**, *39*, 5122−5126.
(40) Zhang, Z.; Ma, H. W.; Hausner, D. B.; Chilkoti, A.; Beebe, T. P. *Biomacromolecules* **2005**, *6*, 3388−3396.
(41) Hyun, J.; Ma, H.; Banerjee, P.; Cole, J.; Gonsalves, K.; Chilkoti, A. *Langmuir* **2002**, *18*, 2975−2979.
(42) Buck, C. A.; Horwitz, A. F. *Annu. Rev. Cell Biol.* **1987**, *3*, 179−205.
(43) Kao, W. J.; D., L.; Schense, J. C.; Hubbell, T. A. *J. Biomed. Mater. Res.* **2001**, *55*, 79−88.
(44) Kao, W. J.; Lee, D. *Biomaterials* **2001**, *22*, 2901−2909.
(45) Benoit, D. S. W.; Anseth, K. S. *Biomaterials* **2005**, *26*, 5209−5220.
(46) Ufret, M. L.; Griffith, L. G. Massachusetts Institute of Technology, Cambridge, MA. To be submitted for publication.
(47) Annunziato, M.; Patel, U.; Ranade, M.; Palumbo, P. *Bioconjugate Chem.* **1993**, *4*, 212−218.
(48) Chan, W. C.; White, P. D. *FMOC Solid Phase Peptide Synthesis*; Oxford University Press: Oxford, 2000.
(49) Markwell, M. A. K. *Anal. Biochem.* **1982**, *125*, 427−432.
(50) Hermanson, G. T. *Bioconjugate Techniques*; Academic Press: San Diego, CA, 1996.
(51) Gordon, G. W.; Berry, G.; Liang, X. H.; Levine, B.; Herman, B. *Biophys. J.* **1998**, *74*, 2702−2713.
(52) Lakowicz, J. R. *Principles of Fluorescence Spectroscopy*, 2nd ed.; Kluwer Acacdemic: New York, 1999.
(53) Puklin-Faucher, E.; Gao, M.; Schulten, K.; Vogel, V. *J. Cell Biol.* **2006**, *175*, 349−360.
(54) Iwasaki, K.; Mitsuoka, K.; Fujiyoshi, Y.; Fujisawa, Y.; Kikuchi, M.; Sekiguchi, K.; Yamada, T. *J. Struct. Biol.* **2005**, *150*, 259−267.
(55) Dubin-Thaler, B. J.; Giannone, G.; Dobereiner, H.-G.; Sheetz, M. P. *Biophys. J.* **2004**, *86*, 1794−1806.
(56) Brinkerhoff, C. J.; Linderman, J. J. *Tissue Eng.* **2005**, *11*, 865−876.
(57) Irvine, D. J.; Hue, K.-A.; Mayes, A. M.; Griffith, L. G. *Biophys. J.* **2002**, *82*, 120−132.
(58) Kong, H. J.; Polte, T. R.; Alsberg, E.; Mooney, D. J. *Proc. Natl. Acad. Sci. U.S.A.* **2005**, *102*, 4300−4305.
(59) Weber, G. *Adv. Protein Chem.* **1975**, *29*, 1−83.
(60) Xiao, Y.; Truskey, G. A. *Biophys. J.* **1996**, *71*, 2869−2884.
(61) Ruoslahti, E. *Annu. Rev. Cell. Dev. Biol.* **1996**, *12*, 697−715.
(62) Mrksich, M. *Chem. Soc. Rev.* **2000**, *29*, 267−273.
(63) Lee, J. H.; Lee, H. B.; Andrade, J. D. *Prog. Polym. Sci.* **1995**, *20*, 1043.

BM070237O